Electron wave collimation by conical horns: computer simulation

1991 J. Phys.: Condens. Matter 3 8247

(http://iopscience.iop.org/0953-8984/3/42/019)

J. Phys.: Condens. Matter 3 (1991) 8247–8256. Printed in the UK

Electron wave collimation by conical horns: computer simulation

K Michielsen and H De Raedt

Institute for Theoretical Physics, University of Groningen, PO Box 800, NL-9700 AV Groningen, The Netherlands

Received 8 March 1991, in final form 1 May 1991

Abstract. Results are presented of extensive numerical simulations of electron wave packets transmitted by horns. A detailed quantitative analysis is given of the collimation of the electron wave by horn-like devices. It is demonstrated that the electron wave collimation effect cannot be described in terms of adiabatic wave expansion and semi-classical considerations. It is argued that, in the context of atomic-size electron beam sources, the collimation effect due to a possible horn-like structure in the metal–vacuum potential is much less than the effect stemming from the tunnel barrier itself.

1. Introduction

Recent experiments on atomic-size tips [1–4] have demonstrated that they act as unusual electron beam sources, emitting electrons at fairly low applied voltages (a few thousand volts or less) with a small angular spread (of a few degrees). These properties make such electron sources very attractive for applications to electron holography and electron interferometry [5–9]. Extensive theoretical work [10, 11] revealed that tunnelling through the metal–vacuum potential is the main physical mechanism determining the unusual properties of the emitted electron beams.

Tunnelling through a potential barrier is only one of the mechanisms for collimating an electron beam. In particular, it has been suggested [12] that adiabatic mode selection [13–15] is mainly responsible for the peculiar properties of the electron beams emitted from atomic-size tips. The key ingredient of this description is the presence of a slowly varying, horn-like structure in the potential surrounding the tip and the assumption that the electron wave propagates adiabatically in this structure. However, the application of these ideas to the atomic-size tips seems unjustified [16].

Recent advances in fabricating quantum point contacts in GaAs heterostructures have opened up the possibility of performing 'electron optics' experiments in solids [17]. A prerequisite is the existence of a large electronic mean free path allowing the electron to move ballistically over a large (relative to the electron wavelength) distance. From the viewpoint of field-electron emission, motion in the vacuum region is replaced by ballistic motion in the solid. Just as for the electron-beam sources, it is of great interest to explore the possibility of focusing (collimating) electrons in the solid [18]. It has been demonstrated that magnetic fields [17–20] or an electrostatic lens [21] can be used to focus the electrons. Furthermore it has been argued [17, 22]

0953-8984/91/428247+10$03.50

that the rounding of the entrance/exit plane of quantum point contact may act as a horn, leading to the collimation of the electron waves.

It is important to recognize that electron waves emitted by atomic-size tips are collimated to a much greater extent (a few degrees) than those produced by quantum point contacts. This is partially due to the presence of the applied electric field which accelerates the electron when it emerges from the tip over a macroscopic distance.

Whether the tunnel barrier or the horn-like structure or both are the dominant mechanism for collimating the electron wave is important for the design of devices in which the spatial dimensions are comparable with the electron wavelength. To investigate this problem on a quantitative level we solve the time-dependent Schrödinger equation (TDSE) for an ideal atomic-size horn and demonstrate that the collimation effect due to the horn is small compared with that of the tunnel barrier. Our calculations also allow us to assess the applicability of the adiabatic approximation [17] used to estimate the collimation factor of a horn.

The problem of calculating the angular distribution of electron waves emitted by an ideal horn closely resembles the one encountered in the design of microwave or millimetre-wave radiating horn-like components [23]. The standard technique for solving the corresponding wave equations is to represent the radiating component as a stepped waveguide and to match the modes at the waveguide step discontinuities, i.e. a *transfer matrix* approach. The numerical method employed in this article differs in many respects. Instead of solving a stationary wave equation we solve the TDSE for a wave packet incident on the throat of the horn and analyse the transmitted wave packet by projecting it onto a screen placed far away (many electron wavelengths) from the emitting aperture. Physically this setup is identical to the one used in experiments on atomic-size tips [1–4]. The TDSE approach can handle arbitrary potentials and therefore does not suffer from limitations on the size of the apertures and the length of the horn. It is numerically stable and convergent under all circumstances [24]. Its main limitation is that, due to memory and CPU requirements, realistic calculations can only be carried out for two-dimensional (2D) systems. However, these 2D models contain all the essential features of their 3D counterparts and therefore physical insight into the processes that govern the emission of the electron wave obtained from the 2D simulations applies to the 3D case as well.

2. Model and simulation technique

The first step is to construct a model, i.e. to specify a potential, that contains the most prominent features of the horn. This model is solved by exact numerical integration of the corresponding time-dependent Schrödinger equation [24]. Analysis of the time development of the wave packets should then allow us to study the collimation effect as a function of the model parameters.

The basic idea is to solve the TDSE

$$i\hbar\frac{\partial\psi(\boldsymbol{r},t)}{\partial t} = \mathcal{H}\psi(\boldsymbol{r},t) \tag{2.1}$$

for a Hamiltonian of the form

$$\mathcal{H} = \frac{p^2}{2m} + V(\boldsymbol{r}). \tag{2.2}$$

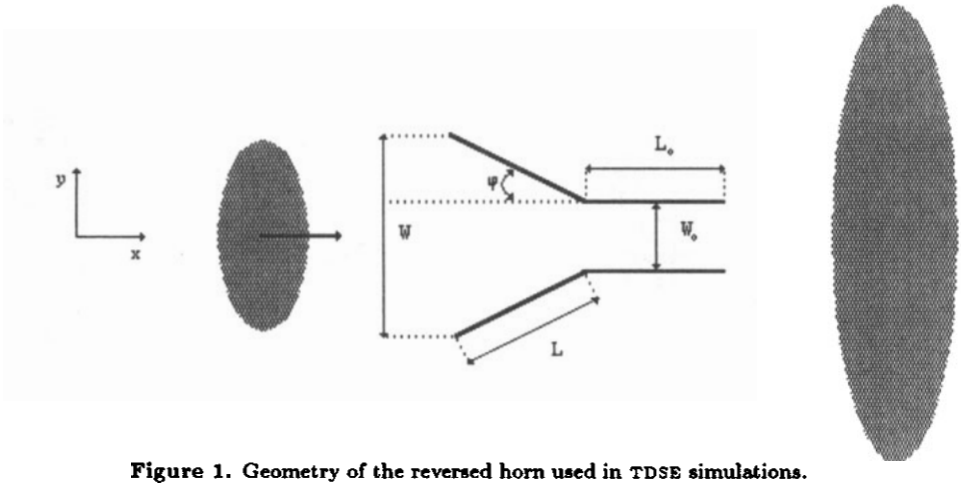

Figure 1. Geometry of the reversed horn used in TDSE simulations.

For practical purposes it is convenient to express distances in units of λ_F, the relevant wavelength of the electron. Wavevectors are then measured in units of $k_F = 2\pi/\lambda_F$, energies in units of $E_F = \hbar^2 k_F^2/2m$, and time in units of $\hbar/E_F$. In these units equations (2.1) and (2.2) read

$$i\frac{\partial\psi(\boldsymbol{r},t)}{\partial t} = \mathcal{H}\psi(\boldsymbol{r},t) \tag{2.3}$$

and

$$\mathcal{H} = -\frac{\nabla^2}{(2\pi)^2} + \frac{V(\boldsymbol{r})}{E_F}. \tag{2.4}$$

The geometry of the model is depicted in figures 1 and 2. A horn is characterized by its smallest width W_0, its length L and its flare angle φ (or its aperture $W = W_0 + 2L\sin\varphi$). To examine the effect of mode selection by a constriction on the transmission properties of a horn we attach a constriction of length L_0 and width W_0 to the horn. For the sake of brevity we will henceforth call this two-component structure a 'horn'. The potential $V(\boldsymbol{r})$ is zero inside the horn and to the left and right of it, and very large ($V(\boldsymbol{r}) = 100E_F$ in practice) otherwise. Our motivation to study this 'ideal' horn instead of a horn in which the shape is a continuous function of the coordinates is twofold. First we can make contact, on a quantitative level, with other numerical work [10, 11], thereby allowing us to compare the effect of different mechanisms for collimating the electron waves. Second, although our simulation technique can handle smoothly changing potentials as easily as discontinuous potentials, the ideal horn studied in this work corresponds to a 'worst-case' situation and therefore yields information on the limiting values of properties such as the collimation factor.

We will consider two different cases: first a wave incident at the largest aperture (figure 1) and second a wave entering the horn at the smallest aperture (figure 2). In many respects these two situations are complementary and therefore provide a consistency check on the simulation results and their interpretation.

A convenient choice for the initial wave packet is

$$\psi(x,y,t=0) \propto e^{ik_F(x\cos\psi + y\sin\psi)} e^{-(x-x_0)^2/2\sigma_x^2} e^{-(y-y_0)^2/2\sigma_y^2} \tag{2.5}$$

i.e. a Gaussian wave packet centred around (x_0, y_0) with a width of $\sigma_x(\sigma_y)$ in the $x(y)$-direction. In free space the wave packet would move in the $(\cos\psi, \sin\psi)$-direction. We

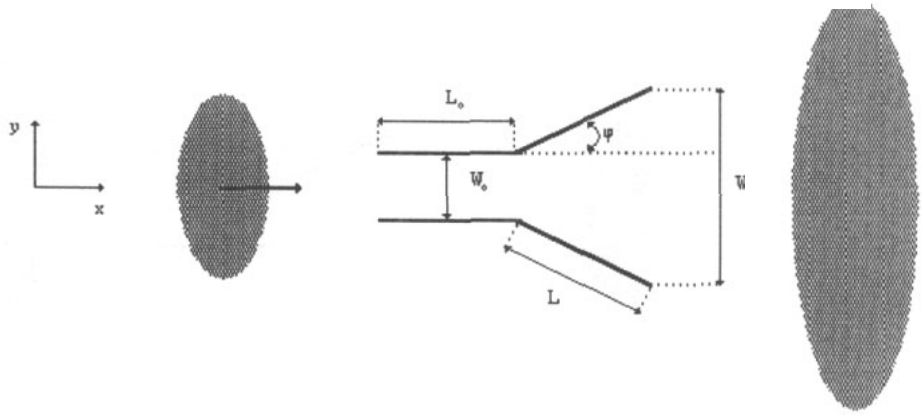

Figure 2. Geometry of the horn used in TDSE simulations.

adopt the convention that the wave packet starts from the left of the horn and moves to the right. In practice the initial wave packet is multiplied by a spatial window so that the probability inside and to the right of the horn is zero.

The simulation consists in following the time evolution of the wave packet. In its most primitive form this means taking snap-shots of the probability distribution at regular time intervals. We simultaneously monitor the total probability transmitted. As a function of time, this probability becomes constant. For all practical purposes we may then regard the transmission of waves through the horn as completed.

To analyse the angular distribution of the transmitted wave packet, we project it onto a screen placed far away from the object under investigation. The main idea is that, once the transmitted wave packet is sufficiently far from the potential, it moves in free space. In the appendix it is shown how to extract the angular distribution from an arbitrary wave packet (subject to a uniform electric field) moving in free space. In practice this amounts to Fourier transforming the transmitted wave packet and performing some integration operations. The resulting angular distribution corresponds to the image seen on the screen, as produced by field-emitted electrons for example.

We end this section by giving some details on the simulation technique itself. In this work we have used a five-point difference formula for $\partial^2/\partial x^2$ (and $\partial^2/\partial y^2$) and a fourth-order real-space product formula to perform the time integration [24]. A spatial mesh size of 10 or 20 lattice points per wavelength λ_F was used. In combination with the five-point difference formula this assures sufficient accuracy, as comparison of results obtained from simulation with $\delta = \lambda_F/10$ and $\delta = \lambda_F/20$ shows. For $\delta = \lambda_F/10$ ($\delta = \lambda_F/20$) the time-step $\tau = 0.03125$ ($\tau = 0.015625$) is small enough to guarantee that systematic errors resulting from the use of the product formula [24] are insignificant. Free boundary conditions (i.e. reflecting boundaries) were adopted. The size of the simulation box was typically $52\lambda_F \times 26\lambda_F$, but was occasionally made larger to accommodate the very large horns ($L = 40\lambda_F$), and sufficiently large to eliminate boundary effects. Fourier transforms of transmitted wave packets were carried out using 512 × 512 lattice points. A typical simulation run (135 200 lattice points, $\delta = \lambda_F/10$, $\tau = 0.03125$ and 3072 time steps) takes about 10 min on the NEC SX-2 computer.

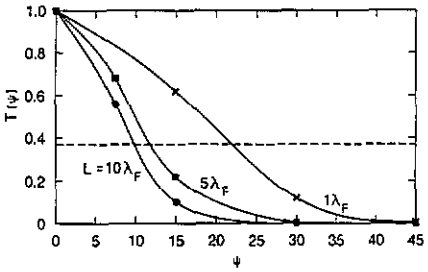

Figure 3. Transmission $T(\psi)$ of a reversed horn as a function of the angle of incidence ψ for various values of the horn length L and $W_0 = \lambda_F$, $L_0 = \lambda_F/2$, $\varphi = 20°$. The value of $T(\psi)$ is normalized to its largest value. The dotted line indicates $T(\psi) = 1/e$.

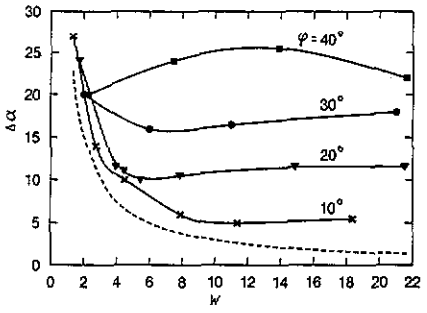

Figure 4. Angular spread $\Delta\alpha$ as a function of the aperture W of the horn, for various values of L, W_0, φ and $L_0 = \lambda_F/2$, $\psi = 0°$.

3. Simulation results

We first consider the reversed horn (figure 1) and concentrate on the influence of the angle of incidence ψ on the transmission $T(\psi)$, for various lengths L of the horn. Due to the reflection symmetry of the horn geometry with respect to the y-direction, $T(\psi) = T(-\psi)$. The angle of incidence $\Delta\psi$ at which the normalized transmission $T(\Delta\psi) = 1/e$ characterizes the angular distribution for incoming waves of the reversed horn.

As shown in figure 3, where $T(\psi)$ is plotted as a function of ψ, $T(\psi)$ decreases with increasing ψ. Making the horns longer reduces $\Delta\psi$. However, the reduction of $\Delta\psi$ is much less in going from horns of length $L = \lambda_F$, where $\Delta\psi = 22°$, to one of length $L = 5\lambda_F$, where $\Delta\psi = 12°$, than in going from horns of length $L = 5\lambda_F$ to one of length $L = 10\lambda_F$, where $\Delta\psi = 10°$. This indicates that $\Delta\psi$ is going to a constant value for very long horns.

Next we consider the horn (figure 2) and investigate the connection between the geometry of the horn and the collimation of the electron wave packet. To characterize the collimation we calculate the angular spread $\Delta\theta$, which is defined as $\Delta\theta \equiv |\theta_1 - \theta_2|$ where $\theta_{1,2}$ are determined such that the normalized angular distribution (see appendix) $P(\theta_{1,2}) = 1/e$. We define $\Delta\alpha \boxminus \Delta\theta/2$, because due to the reflection symmetry of the horn with respect to the y-direction, $P(\theta)$ for a positive value of the angle of incidence ψ equals $P(-\theta)$ for $-\psi$. As our calculations for $\Delta\alpha$ are carried out for a fixed angle of incidence ψ of the wave packet and not some superposition of waves coming from different directions, $\Delta\alpha$ is a lower limit to the angular spread of the electron beam. Our calculations for $\psi \neq 0$ show that, in general, the values for $\Delta\alpha$ do not significantly depend on ψ, although the shape of the angular profile itself does. Therefore we may henceforth confine ourselves to a discussion of results for normal incidence $\psi = 0$.

In figure 4, where $\Delta\alpha$ is shown as a function of the aperture $W = W_0 + 2L\sin\varphi$ of the horn for fixed flare angles φ, it is seen that horns with a large opening at the end are collimating much better than horns with a small opening at the end. However, at a certain aperture W the angular spread becomes constant. The smallest angular

spread is given by horns with a small flare angle φ, as illustrated by the curve for $\varphi = 10°$. This indicates that horns with a large aperture W and a small flare angle φ are good collimators. A horn with a flare angle $\varphi = 40°$ does not focus the wave packet, not even when the horn is made longer. This by itself is no surprise: The angular spread of a wave leaving a constriction (i.e. a horn of length $L = 0$) of width W_0 is approximately 40°, hence a horn having a flare angle of $\varphi = 40°$ will have almost no effect on the expanding wave packet.

The parameters affecting the collimation seem to be W_0, L_0, L and φ. The influence of the geometry of the constriction, i.e. of the length L_0 and the width W_0 of the constriction, on the collimation of the wave packet is small, as shown in table 1. Increasing L_0 by a factor 10 or increasing W_0 by a factor of 4 has no effect on the angular spread $\Delta\alpha$. What remains to be studied in more detail is the influence of φ and L on $\Delta\alpha$. From figure 5, which shows $\Delta\alpha$ as a function of L for constant φ, it follows that long horns (large L) with a small flare angle focus the best, as exemplified by the case $\varphi = 10°$. At a certain length of the horn the angular spread reaches a limiting value. For a horn with length $L = 10\lambda_F$ and flare angle $\varphi = 20°$, this limiting value amounts to $\Delta\alpha = 10°$. Such an effect was already seen in figure 3, where $\Delta\psi = 10°$ for an identical reversed horn. This indicates that $\Delta\alpha$ and $\Delta\psi$ are strongly correlated. Indeed, $\Delta\psi$ characterizes the angular distribution for the incoming wave packet of the reversed horn and $\Delta\alpha$ characterizes the angular distribution for the outgoing wave packet leaving the horn. Finally, we also learn from this figure that horns with a flare angle of $\varphi = 40°$ do not collimate at all (see earlier discussion).

Table 1. Influence of the geometry of the constriction, i.e. of W_0 and L_0, on the angular spread $\Delta\alpha$. We have taken $L = 5\lambda_F$, $\varphi = 20°$ and $\psi = 0°$.

W_0/λ_F	L_0/λ_F	$\Delta\alpha$ (deg)
0.5	0.5	12
1	0.5	11
1	5	11
2	0.5	11

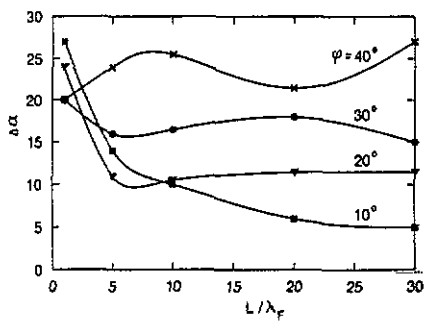

Figure 5. Angular spread $\Delta\alpha$ as a function of the horn length L for various values of the flare angle φ and $W_0 = \lambda_F$, $L_0 = \lambda_F/2$, $\psi = 0°$.

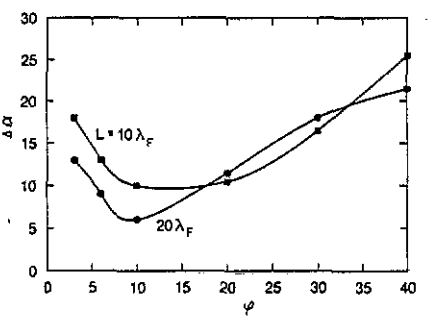

Figure 6. Angular spread $\Delta\alpha$ as a function of the flare angle φ for various values of the horn length L and $W_0 = \lambda_F$, $L_0 = \lambda_F/2$, $\psi = 0°$.

In figure 6, $\Delta\alpha$ is depicted as a function of φ for constant L values. Both curves show a minimum. For $L = 10\lambda_F$, $\Delta\alpha$ reaches a minimum value at $\varphi = 15°$ whereas for $L = 20\lambda_F$, the smallest $\Delta\alpha$ is obtained for $\varphi = 10°$. This again illustrates that long horns with a small flare angle are good collimators. However, the optimal values of L and φ are strongly correlated: For each length L there exists a flare angle φ such that $\Delta\alpha$ is minimal.

4. Discussion

Having presented the results of our simulations, we now want to explore the extent to which they can be understood in terms of simple theoretical models. From Fraunhofer diffraction theory, it follows that the intensity function for diffraction by a slit of width W reads

$$I(p) \sim \left(\frac{\sin(pk_F W/2)}{pk_F W/2}\right)^2 \tag{4.1}$$

where $k_F = 2\pi/\lambda_F$ and $p = \sin\psi' - \sin\psi$. Here ψ denotes the angle of incidence of the wave and ψ' the direction of observation. To make contact with the definition for $\Delta\alpha$ we take $\psi' = \Delta\alpha$ and set $I(p) = 1/e$. This occurs at $p = 0.52\lambda_F/W$, from which

$$\Delta\alpha = \arcsin\frac{0.52\lambda_F}{W_0 + 2L\sin\varphi} \tag{4.2}$$

for normal incidence of the wave packet ($\psi = 0°$) and for $W = W_0 + 2L\sin\varphi$. This theoretical connection between $\Delta\alpha$ and W is included in figure 4 (dotted curve), where $\Delta\alpha$ is shown as a function of the aperture $W = W_0 + 2L\sin\varphi$ of the horn. From figure 4 it is seen that the collimation effect cannot be simply described by diffraction by a slit. A formula for $\Delta\alpha$ similar to (4.2) was derived by Van Houten *et al* [17]. Invoking semi-classical arguments they estimate the collimation factor of the horn, assuming adiabatic invariance of the product of the channel width W and the absolute value of the transverse electron momentum $\hbar k_y$, i.e. of the quantity $S = |\hbar k_y|W$. At the horn entrance the largest possible value of S (in our units) is

$$S_1 = \frac{2\pi}{\lambda_F} W_{\min}. \tag{4.3}$$

Assuming that adiabatic transport holds up to a point of maximal width $W_{\max}$ [17], the largest possible value of S at the horn exit is

$$S_2 = \frac{2\pi}{\lambda_F} W_{\max}\sin\alpha_{\max}. \tag{4.4}$$

Here $W_{\min}$ ($W_{\max}$) denotes the minimum (maximum) width of the horn structure and $2\alpha_{\max}$ is the width of the injection/acceptance cone. Adiabatic invariance of S implies that $S_1 = S_2$, so that

$$\alpha_{\max} = \arcsin\left(W_{\min}/W_{\max}\right). \tag{4.5}$$

To establish the connection to our notation we set $W_{\min} = W_0$, $W_{\max} = W_0 + 2L\sin\varphi$ and $\alpha_{\max} = \Delta\alpha$. This results in

$$\Delta\alpha = \arcsin\left(\frac{W_0}{W_0 + 2L\sin\varphi}\right). \tag{4.6}$$

This expression for $\Delta\alpha$ is indeed very closely related to that in equation (4.2). For $W_0 = \lambda_F$ both formulae are exactly the same, the factor 0.52 not being taken into account. This implies that for $W_0 = \lambda_F$ the collimation effect cannot be described by equation (4.6), as indicated by the dotted curve in figure 4. From equation (4.6) it is seen that the angular distribution $\Delta\alpha$ has to depend on the width W_0 of the constriction which, as shown in table 1, is not the case.

We now turn to the applicability of the adiabatic approximation (slowly varying width of the horn). From geometrical considerations the largest x-value for which the adiabatic approximation is valid follows from [14, 15].

$$\mathrm{d}'(x_c) \leqslant \frac{\pi}{4}\frac{\pi}{2d(x_c)k_F} \tag{4.7}$$

where d' is the derivative of d with respect to x and $2d$ is the width of the aperture of the horn. In our notation, $d(x) = W_0/2 + x\tan\varphi$ and $x_c = L_c\cos\varphi_c$, which results in

$$L_c \leqslant \left(\frac{\pi}{8\tan\varphi_c} - W_0\right)/2\sin\varphi_c. \tag{4.8}$$

Taking $W_0 = \lambda_F$ and $\varphi_c = 10°$ gives $L_c \leqslant 3.5\lambda_F$. For $\varphi_c = 20°$ we find $L_c \leqslant 0.1\lambda_F$. As seen from figure 5, there is very little collimation for such short horns. Collimation occurs for much longer horns ($L \gg \lambda_F$), but then, according to equation (4.8), the adiabatic approximation is no longer valid. Clearly, the collimation effect for long horns cannot be described by the adiabatic approximation.

5. Conclusions

We have presented the results of extensive numerical simulations of electron wave packets transmitted by horns. A detailed quantitative analysis of the collimation of the electron wave by horn-like devices has demonstrated that the collimation effect cannot be described in terms of adiabatic wave expansion and semi-classical considerations. Our results allow us to assess the relative importance of horn-like structures in the metal–vacuum potential of atomic-size electron sources for the strong electron focusing observed experimentally. From all our figures it is clear that to get appreciable collimation the horn should at least be $5\lambda_F$. On the other hand the width of the metal–vacuum tunnel barrier surrounding the atomic-size tip is of the order of λ_F and our calculations do not reveal significant collimation for such short horns. The conclusion must be that for atomic-size electron sources the tunnel barrier is the dominant mechanism for collimating the electrons [10].

Acknowledgments

It is a pleasure to thank T Schneider for his kind hospitality at the IBM Research Laboratories, Zurich. We would like to thank N García, J Imry, A Baratoff and S Ciraci for stimulating discussions. This work is part of the research programme of the Stichting voor fundamenteel Onderzoek der Materie (FOM), which is financially supported by the Nederlandse organisatie voor wetenschappelijk onderzoek (NWO). Some of the simulations were carried out using a grant from the Stichting Nationale Computer Faciliteiten (NCF) and is partially supported by the EEC Science Plan contract SC1-0395-C (MB).

Appendix

Here we derive the expression for the angular distribution on a screen placed far away from the source (the horn in the present case) that produced the wave packet. We assume that once the wave packet has been emitted, it moves in a uniform electric field. The Hamiltonian describing the motion of the wave packet reads

$$\mathcal{H} = \frac{p^2}{2m} - E_0 x \qquad E_0 \geqslant 0. \tag{A1}$$

To compute the time development of the wave packet we first decompose the propagator as

$$\begin{aligned}\exp\left(\frac{-it\mathcal{H}}{\hbar}\right) &\equiv \exp\left[\frac{-it}{\hbar}\left(\frac{p^2}{2m} - E_0 x\right)\right] \\ &= \exp\left(-\frac{it^3E_0^2}{24\hbar m}\right)\exp\left(\frac{itxE_0}{2\hbar}\right)\exp\left(-\frac{itp^2}{2\hbar m}\right)\exp\left(\frac{itxE_0}{2\hbar}\right).\end{aligned} \tag{A2}$$

This representation is exact. The value of the wavefunction $\psi(\boldsymbol{r},t)$ at position $\boldsymbol{r}$ and time t is given by

$$\begin{aligned}\psi(\boldsymbol{r},t) &= \langle \boldsymbol{r}|e^{-it\mathcal{H}/\hbar}|\psi(\boldsymbol{r},t=0)\rangle \\ &= \frac{m}{2\pi i\hbar t}e^{-it^3E_0^2/24\hbar m}\int d\boldsymbol{r}'\, e^{-itxE_0/2\hbar}e^{im(\boldsymbol{r}-\boldsymbol{r}')^2/2\hbar t}e^{itx'E_0/2\hbar}\psi(\boldsymbol{r}',t=0).\end{aligned} \tag{A3}$$

from which

$$\begin{aligned}|\psi(\boldsymbol{r},t)|^2 = \left(\frac{m}{2\pi\hbar t}\right)^2 \int d\boldsymbol{r}'\, d\boldsymbol{r}''\, e^{it(x'-x')E_0/2\hbar}e^{im(\boldsymbol{r}'-\boldsymbol{r}')(\boldsymbol{r}-(\boldsymbol{r}'+\boldsymbol{r}')/2)/\hbar t} \\ \times \psi^*(\boldsymbol{r}'',t=0)\psi(\boldsymbol{r}',t=0).\end{aligned} \tag{A4}$$

We are interested in the situation in which the distance (x) between the origin and the screen is very large (macroscopic) compared with the spatial extent of the wave packet at $t=0$. Then it is safe to assume $|\boldsymbol{r}| \gg |\boldsymbol{r}'+\boldsymbol{r}''|/2$ as the integration over $\boldsymbol{r}'$ and $\boldsymbol{r}''$ are over a microscopic region of space. Then (A4) reduces to

$$|\psi(\boldsymbol{r},t)|^2 = \left(\frac{m}{2\pi\hbar t}\right)^2 \int d\boldsymbol{r}'\, d\boldsymbol{r}''e^{ix'(mx/\hbar t - tE_0/2\hbar)}e^{imyy'/\hbar t}\psi^*(\boldsymbol{r}'+\boldsymbol{r}'',t=0)\psi(\boldsymbol{r}'',t=0) \tag{A5}$$

which by the convolution theorem is directly related to the Fourier transformed wavefunction, i.e.

$$|\psi(\mathbf{r},t)|^2 \propto t^{-2}\left|\tilde{\psi}\left(q_x=\frac{mx}{\hbar t}-\frac{tE_0}{2\hbar},q_y=\frac{my}{\hbar t},t=0\right)\right|^2 \tag{A6}$$

where we have dropped all irrelevant constants.

The normalized angular distribution at the screen is given by

$$P(\theta)=\frac{\int_0^T \mathrm{d}t\,|\psi(x,y,t)|^2}{\int_0^T \mathrm{d}t\,|\psi(x,y=0,t)|^2} = \frac{\int_0^\infty \mathrm{d}q_x(1+q_x/\sqrt{q_x^2+V^2})|\tilde{\psi}(q_x,q_y=0.5(q_x+\sqrt{q_x^2+V^2})\tan\theta,t=0)|^2}{\int_0^\infty \mathrm{d}q_x(1+q_x/\sqrt{q_x^2+V^2})|\tilde{\psi}(q_x,q_y=0,t=0)|^2} \tag{A7}$$

where V denotes the applied voltage (in units of volts) and $\tan\theta = y/x$. For the case at hand we have given all the expressions in two dimensions, extension to higher dimensions being trivial.

References

[1] Fink H-W 1986 *IBM J. Res. Dev.* **30** 460
[2] Fink H-W 1988 *Phys. Ser.* **38** 260
[3] Binh Vu Thien and Marien J 1988 *Surf. Sci.* **102** L539
[4] Binh Vu Thien 1988 *J. Microsc.* **152** 355
[5] Gabor D 1949 *Proc. R. Soc.* A **454** 197
[6] Gabor D 1951 *Proc. R. Soc.* B **64** 449
[7] Tonomura A 1987 *Rev. Mod. Phys.* **59** 639
[8] Lichte H 1986 *Ultramicroscopy* **20** 293
[9] Missiroli F G, Pozzi G and Valdre U 1981 *J. Phys. E: Sci. Instrum.* **14** 649
[10] García N, Sáenz J J and De Raedt H 1989 *J. Phys.: Condens. Matter* **1** 9931
[11] Sáenz J J, García, Binh Vu Thien and De Raedt H 1990 *Scanning Tunneling Microscopy and Related Methods* ed R J Behn *et al* (Dordrecht: Kluwer) pp 409–41
[12] Lang N D, Yacobi A and Imry Y 1989 *Phys. Rev. Lett.* **63** 1499
[13] Glazman L I, Lesovik G B, Khmel'nitskii D E and Shekhter R I 1988 *Sov. Phys.-JETP Lett.* **48** 238
[14] Yacobi A and Imry Y 1990 *Europhys. Lett.* **11** 663
[15] Yacobi A and Imry Y 1990 *Phys. Rev.* B **41** 5341
[16] Tekman E, Ciraci S and Baratoff A 1991 *Phys. Rev.* B **43** 7145
[17] van Houten H, Beenakker C W J and van Wees B J 1990 *Semiconductors and Semimetals* ed M A Reed (New York: Academic) at press
[18] Washburn S 1990 *Nature* **343** 415
[19] Baranger H U and Stone A D 1989 *Phys. Rev. Lett.* **63** 414
[20] van Houten H, Beenakker C W J, Williamson J G, Broekaart M E I, van Loosdrecht P H M, van Wees B J, Mooij J E, Foxon C T and Harris J J 1989 *Phys. Rev.* B **39** 8556
[21] Sivan U, Heiblum M, Umbach C P and Shtrikman H 1990 *Phys. Rev.* B **41** 7937
[22] Beenakker C W J and van Houten H 1989 *Phys. Rev.* B **39** 10445
[23] Wreidt T, Wolff K-H, Arndt F and Tucholke U 1989 *IEEE Trans.* **AP-37** 780
[24] De Raedt H 1987 *Comput. Phys. Rep.* **7** 1